Two-photon intravital imaging of lungs during anthrax infection reveals long-lasting macrophage-dendritic cell contacts.

Daniel Fiole, Pierre Deman, Yannick Trescos, Jean-François Mayol, Jacques Mathieu, Jean-Claude Vial, Julien Douady, Jean-Nicolas Tournier

zii00214/zii0521d14z | xppws | S=1 | 12/11/13 | 10:34 | 4/C Fig: 1,2,3,4,5,6 | ArtID: 01184-13 | NLM: research-article | CE: jtc

Editor: Blanke | Section: Host Response and Inflammation | Designation: T

IAI Journals.ASM.org

Two-Photon Intravital Imaging of Lungs during Anthrax Infection Reveals Long-Lasting Macrophage-Dendritic Cell Contacts

AQ: au Daniel Fiole,[a,b]* Pierre Deman,[a] Yannick Trescos,[a] Jean-François Mayol,[c] Jacques Mathieu,[a,d] Jean-Claude Vial,[b] Julien Douady,[b] Jean-Nicolas Tournier[a,d,e]

AQ: aff Unité Interactions Hôte-Agents pathogènes, Institut de Recherche Biomédicale des Armées, Brétigny-sur-Orge, France[a]; Laboratoire Interdisciplinaire de Physique, UMR 5588 CNRS/Université Joseph Fourier Grenoble 1, St-Martin-d'Hères, France[b]; Unité de Radiobiologie Tissulaire, Institut de Recherche Biomédicale des Armées, Brétigny-sur-Orge, France[c]; Laboratoire Pathogénie des Toxi-Infections Bactériennes, Institut Pasteur, Paris, France[d]; Ecole du Val-de-Grâce, Paris, France[e]

The dynamics of the lung immune system at the microscopic level are largely unknown because of inefficient methods of restraining chest motion during image acquisition. In this study, we developed an improved intravital method for two-photon lung imaging uniquely based on *a posteriori* parenchymal tissue motion correction. We took advantage of the alveolar collagen pattern given by the second harmonic generation signal as a reference for frame registration. We describe here for the first time a detailed dynamic account of two major lung immune cell populations, alveolar macrophages and CD11b-positive dendritic cells, during homeostasis and infection by spores of *Bacillus anthracis*, the agent of anthrax. We show that after alveolar macrophages capture spores, CD11b-positive dendritic cells come in prolonged contact with infected macrophages. Dendritic cells are known to carry spores to the draining lymph nodes and elicit the immune response in pulmonary anthrax. The intimate and long-lasting contacts between these two lines of defense may therefore coordinate immune responses in the lung through an immunological synapse-like process.

The lung is a crucial and yet very delicate organ dedicated to gas exchange through a thin alveolar-capillary wall (1). The obscure side of this highly efficient system is the constitutive fragility of its extensive exchange surfaces. The *tour de force* of the lung-associated immune system consists of its innate ability to protect against infection and pollutants while maintaining an anti-inflammatory environment (2). This complicated balance is achieved by a network of scattered cells such as alveolar macrophages on the outer side of the alveoli and different subsets of interstitial dendritic cells (DCs) (3).

Recent advances in intravital microscopy (IVM) using two-photon excitation fluorescence (TPEF) have profoundly improved our understanding of the immune system dynamics in most organs, except the lungs (4). A detailed account of host-pathogen interactions in diverse tissues has been given (5–11), but lung immune system investigation by IVM has lagged due to the lack of a noninvasive and effective method taking into account lung features.

Recent studies have addressed rigorous lung parenchyma IVM using TPEF in inflammation models (12). Two alternative *a priori* stabilization methods have been used by others to restrain movement compatible with imaging, based either on gluing the parenchyma onto a frame (13) or on a suction system stabilizing the lung under a glass window (14). These techniques, although effective for various purposes, are not optimal, as they alter the physiological motion of the parenchyma and may provoke unexpected reactions.

We describe here an alternative approach for studying the lung by IVM based uniquely on *a posteriori* tissue motion correction. We take advantage of the fibrillar collagen pattern given by second harmonic generation (SHG) signals as a reference for frame registration and removal of wobbling images. This method allows acquisition in two spatial dimensions of immune cell dynamics in the lung of anesthetized mice, without any chest mechanical stabilization. While previous studies of the lungs have mainly focused on microvascularization (14) and/or inflammation (13, 15), we describe here for the first time dynamic cross talk between two major immune cell populations (macrophages and DCs) after infection by *Bacillus anthracis*, the causative agent of anthrax that affects livestock and humans.

B. anthracis infection through the lungs causes a fulminant infection (16). Lung DCs transport inhaled spores to lymph nodes, where germination occurs and gives rise to septicemia, toxemia, and rapid death (2, 17). In the lung at the cellular level, we have previously shown that on the one hand alveolar macrophages capture spores within minutes, while on the other hand conventional CD11b CX3CR1 DCs take over after 30 min and transport spores to the lymph nodes (18, 19). At that time, no link between these phenomena had been established.

Here, we dissect the early steps of *B. anthracis* pulmonary infection by using an improved lung IVM method in conjunction with TPEF and SHG. In this paper, we show for the first time that the response to infection includes scanning of macrophage surfaces by DCs expressing the CX3CR1 fractalkine receptor. This process not only could embody the missing link to the comprehension of spore sampling at the lung level in anthrax infection

Received 20 September 2013 **Returned for modification** 2 November 2013
Accepted 2 December 2013

Published ahead of print 9 December 2013

Editor: S. R. Blanke

Address correspondence to Jean-Nicolas Tournier, jntournier@gmail.com.

* Present address: Daniel Fiole, Department of Neurology, David Geffen School of Medicine at the University of California, Los Angeles, California, USA.

Supplemental material for this article may be found at http://dx.doi.org/10.1128/IAI.01184-13.

doi:10.1128/IAI.01184-13

but, more generally, might lead to a better coordination of the immune response following bacterial infection through an immunological synapse-like mechanism.

MATERIALS AND METHODS

Animal care. All experimental procedures were performed in accordance with governmental guidelines for the care and use of laboratory animals and were also approved by our institutional ethics committee. CX3CR1$^{+/gfp}$ mice, also referred to as CX3CR1 mice (Jackson Laboratory, Bar Harbor, MA), and Flk-1^{gfp} mice (obtained from J.-L. Thomas, INSERM, Paris, France) were maintained under pathogen-free conditions (Institut Jean Roget, La Tronche, France). During studies, mice were anesthetized by the use of 20% Ketamine 1000 (Virbac, Carros, France) plus 5% Rompun (Bayer Healthcare GA, Monheim, Germany) diluted in sterile phosphate-buffered saline (PBS) that was injected intraperitoneally. All efforts were made to minimize animal suffering.

Staining and infection of *Bacillus anthracis* spores. Avirulent *B. anthracis* Sterne 7702 strain spores were chemically labeled with Alexa Fluor 568 or 633 (Invitrogen Life Technologies, Carlsbad, CA) following a method previously published (18). Mice were surgically administered either 10^8 spores per mouse or PBS (50 μl) via an intratracheal flexible cannula.

Imaging setup. TPEF imaging was performed on a Zeiss LSM 710 NLO microscope equipped with a W Plan-Apochromat 20× numerical aperture (NA) 1.0 differential inference contrast (DIC) M27 75-mm water immersion objective. Excitation was produced at 854 nm by a tunable pulsed laser (Chameleon; Coherent, Santa Clara, CA). SHG was epicollected by a dedicated nondescanned detector (NDD) coupled with a 427- ± 20-nm bandpass filter, green fluorescent protein (GFP) by a 500-to-550-nm NDD, rhodamine B or Alexa Fluor 568 by a 565-to-610-nm NDD, and Alexa Fluor 633 by a 660-to-730-nm NDD (see Fig. S1A in the supplemental material). z-stacks are rendered using a maximum-intensity projection.

***In situ* experiments.** Lung explants were bisected with a vibratome (Leica). Samples were glued onto a petri dish filled with 37°C RPMI medium (minus phenol red) using Vetbond (3M Co., Maplewood, MN) (20). Sample drift was corrected using a strategy previously described (21).

Macrophage staining and flow cytometry. Five hours prior to the experiments, mice were intranasally administered 500 μg of rhodamine B-dextran or fluorescein isothiocyanate (FITC)-dextran (10 kDa) diluted in 30 μl of warm PBS (22). Bronchoalveolar lavage (BAL) fluids and lung-derived cells were collected. Cells were incubated with phycoerythrin-labeled anti-CD11b and allophycocyanin-labeled anti-CD11c antibodies (BD Biosciences, Le Pont de Claix, France). After 45 min incubation at 4°C, cells were washed and resuspended in a Hoechst 33258 solution prior to analysis. Cells were analyzed on a LSR II flow cytometer (BD Biosciences, Franklin Lakes, NJ) and data interpreted with Flowjo software (Treestar, Ashland, OR). All interpretations were performed after doublet and dead cell exclusion.

Surgical preparation for *in vivo* imaging. Anesthetized mice were placed in the right lateral decubitus position under a flexiVent mechanical ventilator (SCIREQ Inc., Montreal, Canada) and ventilated at 120 breaths per minute with 2 cm of H_2O positive end-expiratory pressure. Two to three ribs were surgically removed, revealing the left, anterior lung surface (14, 20). A 12-mm-diameter glass coverslip was placed upon the resected ribs and gently maintained using a window system adapted from a previous study (23) (see Fig. S1B in the supplemental material). Care was taken not to limit lung motion due to ventilation.

RESULTS

***In vivo* image postprocessing.** In order to overcome *a posteriori* chest motion occurring during image acquisition, our strategy aimed at (i) acquiring an *in vivo* high-rate series of images after surgery but without mechanical stabilization of the lung and (ii) extracting only one image every minute within each series so as to get rid of wobbling images due to tissue motion.

Five-second TPEF imaging sequences were performed every minute on a living mouse at 10 frames per second, resulting in the acquisition of fluorescent markers of cells (GFP for CX3CR1-DCs) and of second harmonic generation (SHG) signal from fibrillar collagen in the lung, which provides information on alveolar structures. In the resulting time series, most of the images show important deformations due to thoracic motion. One image exhibiting no deformation was chosen. The collagen pattern coming from SHG (Fig. 1A) was then used as a frame of reference for the following image registration phase.

The normalized two-dimensional (2D) cross-correlation coefficient between the frame of reference and every single SHG frame was computed using Matlab (Mathworks, Natick, MA). The frame maximizing this coefficient was extracted in each time series (Fig. 1B). The residual (x, y) drift was corrected using a rigid estimation of the transformation between the selected frames (21, 24) (Fig. 1C) (see Video S3 in the supplemental material, showing the results of an experiment performed on a naive CX3CR1 mouse).

We further tested if our procedure could induce a vascular leak, which would have indicated lung lesions, as previously shown (14). Flk1^{gfp} mouse were ventilated for 2 h and injected intravenously with rhodamine B-dextran (70 kDa). The mice were then used for *in vivo* imaging with an adapted procedure using the GFP for the frame of reference. We could not detect any extravascular leak of rhodamine B-dextran (70 kDa) (see Fig. S1A; see also Video S4 in the supplemental material).

***In vivo* imaging of spore-DC contacts.** We applied this method to *in vivo* imaging of the lung of CX3CR1 mice 5 h after infection by *B. anthracis* spores (Fig. 2A; see also Videos S5 and S6 in the supplemental material). We selected this time as we had previously shown by running *in situ* experiments that it was appropriate for imaging the capture of spores (19). *In vivo* time-lapse experiments showed spores close to CX3CR1-dendritic-like cells spread on the collagen grid. We and others have previously shown that DCs could be differentiated via their roundness coefficient (15, 21). By using the instantaneous roundness coefficient defined as a normalized ratio between area and perimeter, we could assess that those cells were mostly CX3CR1-DCs (Fig. 2B). In contrast to our expectations, we saw only scarce events of direct spore capture by CX3CR1-DCs (20). A closer analysis of spore movements along the DCs clearly revealed a synchronous movement of at least two spores along the CX3CR1-DC (Fig. 2C, red and white tracks). As spores do not have any means to move by themselves, we hypothesized that those spores were already phagocytized in an unstained cell of a different lineage in close contact to a CX3CR1-DC. The most efficient phagocytes in the lung are alveolar macrophages, which at this stage represent the best candidate for this cell making contact with CX3CR1-DCs *in vivo*. Some images taken later revealed a large amount of spores packed in phagosomes of unstained cells very close to CX3CR1-DCs (Fig. 2D and E). Taken together, all these data imply CX3CR1-DC and macrophage contacts in the lung *in vivo*.

***In vivo* imaging of macrophage and DC behaviors.** We administered FITC-dextran to CX3CR1 mice by an intranasal route before infection to perform *in vivo* staining of macrophages (22). We checked by flow cytometry that a large majority of dextran-loaded cells exhibited a phenotype of CD11b-negative CD11c-positive macrophages in the total lung population (99%) and in

zii00214/zii0521d14z | xppws | S=1 | 12/11/13 | 10:34 | 4/C Fig: 1,2,3,4,5,6 | ArtID: 01184-13 | NLM: research-article | CE: jtc

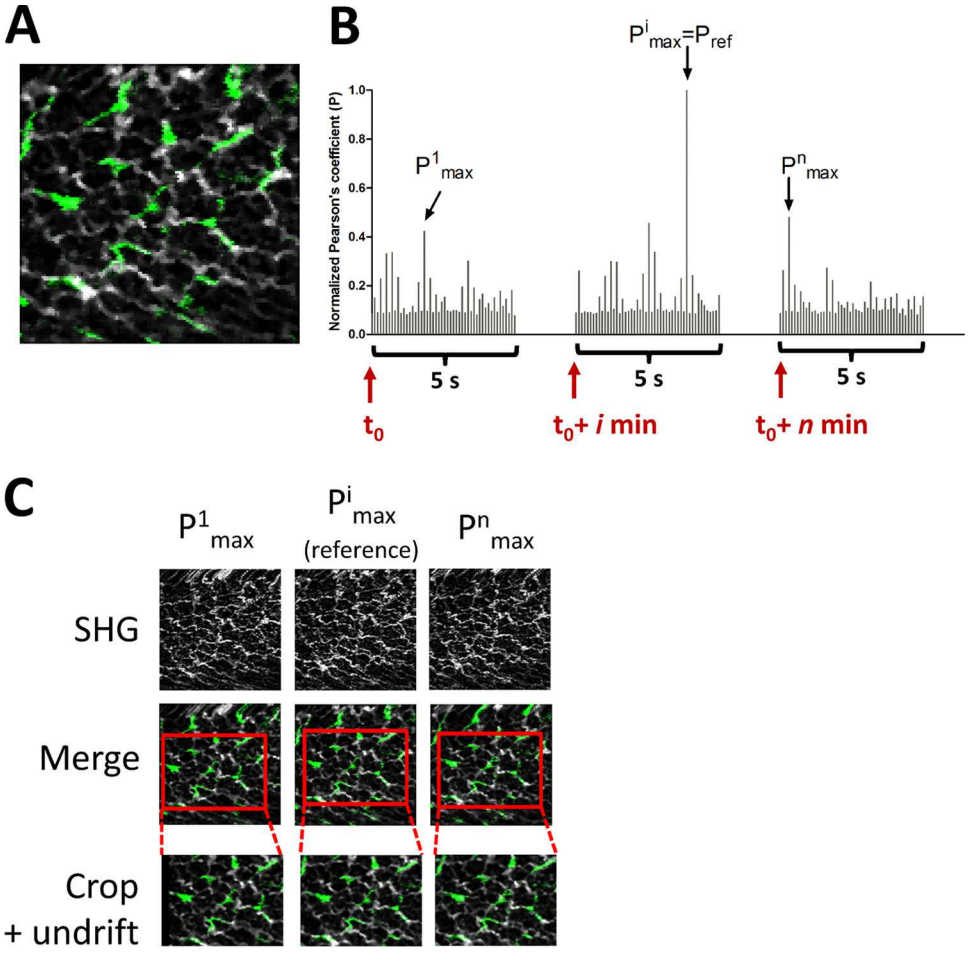

COLOR

FIG 1 Postprocessing applied to a naive CX3CR1 mouse. (A) Example of a reference frame. (B) Five-second sequences of acquisition are performed every minute, resulting in 50 frames in each time series. The 2D cross-correlation coefficient between the collagen pattern of the reference frame (gray) and every frame from the 1st to the *n*th 5-s time series was computed, and the frame maximizing this coefficient was selected in each time series. (C) The residual (*x* and *y*) drift was corrected by estimation of the rigid transformation parameters using comparison of their collagen patterns (SHG). Green, CX3CR1 cells (GFP); gray, fibrillar collagen (SHG) (see Video S3 in the supplemental material).

F3 bronchoalveolar lavages (95%) (Fig. 3A). For microscopy experiments, we used rhodamine B-dextran instead of FITC-dextran as the FITC detector was used for GFP of CX3CR1 cells. This four-color TPEF *in situ* imaging setting allowed us to discriminate the specific signal from macrophages that colocalized with Alexa-stained spores after infection (Fig. 3B). Interestingly, after infection we observed macrophages filled with spores intermingled with DCs.

Infection enhances contacts between macrophage and CX3CR1-DC. Interestingly, we observed a significant increase of the contact ratio induced by *B. anthracis* spores (Fig. 3C). As infection induces recruitment of different cell populations, including CX3CR1-monocytes in the lung, we compared the contact numbers by using a normalized ratio not affected by the recruitment of one or both of these populations. This normalized ratio was defined as the number of contacts divided by macrophage and CX3CR1 cell numbers. The normalized ratio of contact was calculated as an average of 10 randomly chosen *in situ* images (200 μm by 200 μm by 100 μm) from the same mouse. To avoid taking into account false positives, Z-stacks were not projected. The increase of contacts was not correlated with an increase of mean cell velocity in both CX3CR1 cells and macrophages at 5 h postinfection (Fig. 3D).

Dynamic imaging of macrophage-CX3CR1-DC contacts. By analyzing the dynamics of macrophage and DC contacts by performing *in situ* imaging under conditions favorable for preserving cell dynamics, we observed that contacts were related to movements of both CX3CR1 cells to macrophages (Fig. 4A and B; see F4 also Videos S7 and S8 in the supplemental material) and macrophages to CX3CR1 cells. We observed that the linear velocity of the DC involved in a contact with a macrophage increased from 0.19 μm/min during contact to 0.72 μm/min immediately after contact (Fig. 4B). Even though macrophages may transfer spores or antigenic material to CX3CR1-DCs, as suggested by previous *in vitro* work (25), we could neither observe such a transfer nor rule out that possibility, as infected macrophages appeared to be in close contact with DCs (Fig. 5A; see also Video S9 in the supple- F5 mental material) and with infected CX3CR1 cells (Fig. 5B). In several instances, CX3CR1 cells behaved *in situ* as scanning the surface of the macrophages over time (up to 30 min), compatible with exchanges of information between cells.

Eventually, we observed CX3CR1-DC and macrophage con-

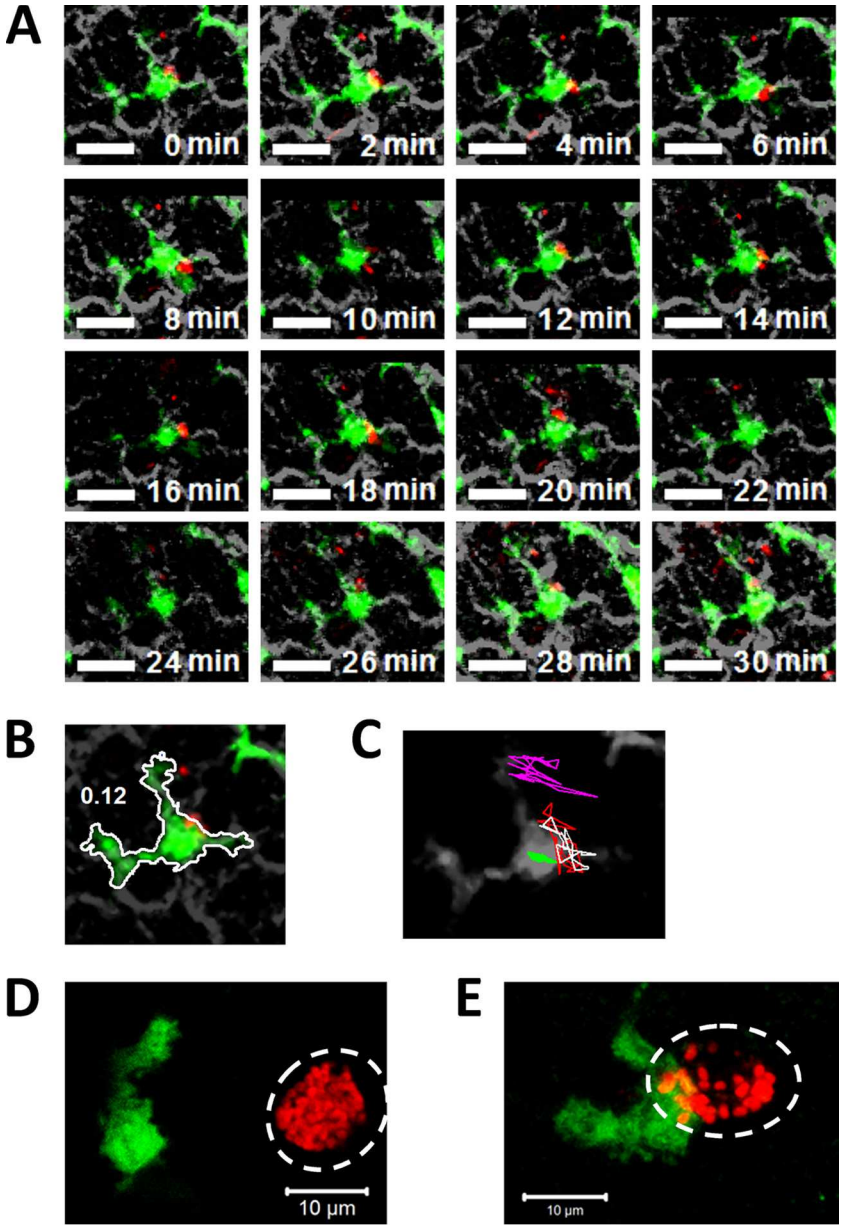

COLOR

FIG 2 TPEF lung *in vivo* imaging of an anthrax-infected CX3CR1 mouse. (A) Time-lapse images of CX3CR1 cell and *B. anthracis* spore interactions during 30 min (see Video S4 in the supplemental material). Bars, 10 μm. (B) Edge of the CX3CR1 cell (white line) showing an instantaneous roundness coefficient equal to 0.12. (C) Tracking of three spores (purple, white, and red lines) and of the CX3CR1 cell (green line) during the experiment. Green, CX3CR1 cells (GFP); red, *B. anthracis* spores (Alexa Fluor 568); gray, fibrillar collagen (SHG). (D and E) Projection of TPEF z-stacks performed *in situ* on a CX3CR1 mouse, 18 h after infection. Green, CX3CR1 cells (GFP); red, *B. anthracis* spores (Alexa Fluor 568).

tacts during *in vivo* experiments performed on infected mice. We observed that contacts could occur *in vivo* over a period as long as 15 min (Fig. 6; see also Video S10 in the supplemental material), suggesting that significant signals may be exchanged between those two cells during that time.

F6

DISCUSSION

Intravital microscopy of the lung from live rodents (i.e., mice) has been achieved only minimally during the past decade due to tissue motion coming from both breathing and heartbeat movements (12, 26). So far, the only way to overcome this major obstacle has been by mechanically stabilizing the lung. While gluing the parenchyma (13) or generating a negative pressure between the organ and a glass window (14, 15, 20) could lead to observations of cell behavior during an inflammatory stimulus or asthma, to our knowledge nothing has been published concerning the immune response in lungs following infection.

In our study, we have not only demonstrated that mechanical stabilization of the lung to achieve IVM is dispensable, but we have also provided novel insights into the triangular interactions between *B. anthracis* spores, macrophages, and DCs. Our results reveal, for the first time, *in vivo* long-lasting contacts between

zii00214/zii0521d14z | xppws | S=1 | 12/11/13 | 10:34 | 4/C Fig: 1,2,3,4,5,6 | ArtID: 01184-13 | NLM: research-article | CE: jtc

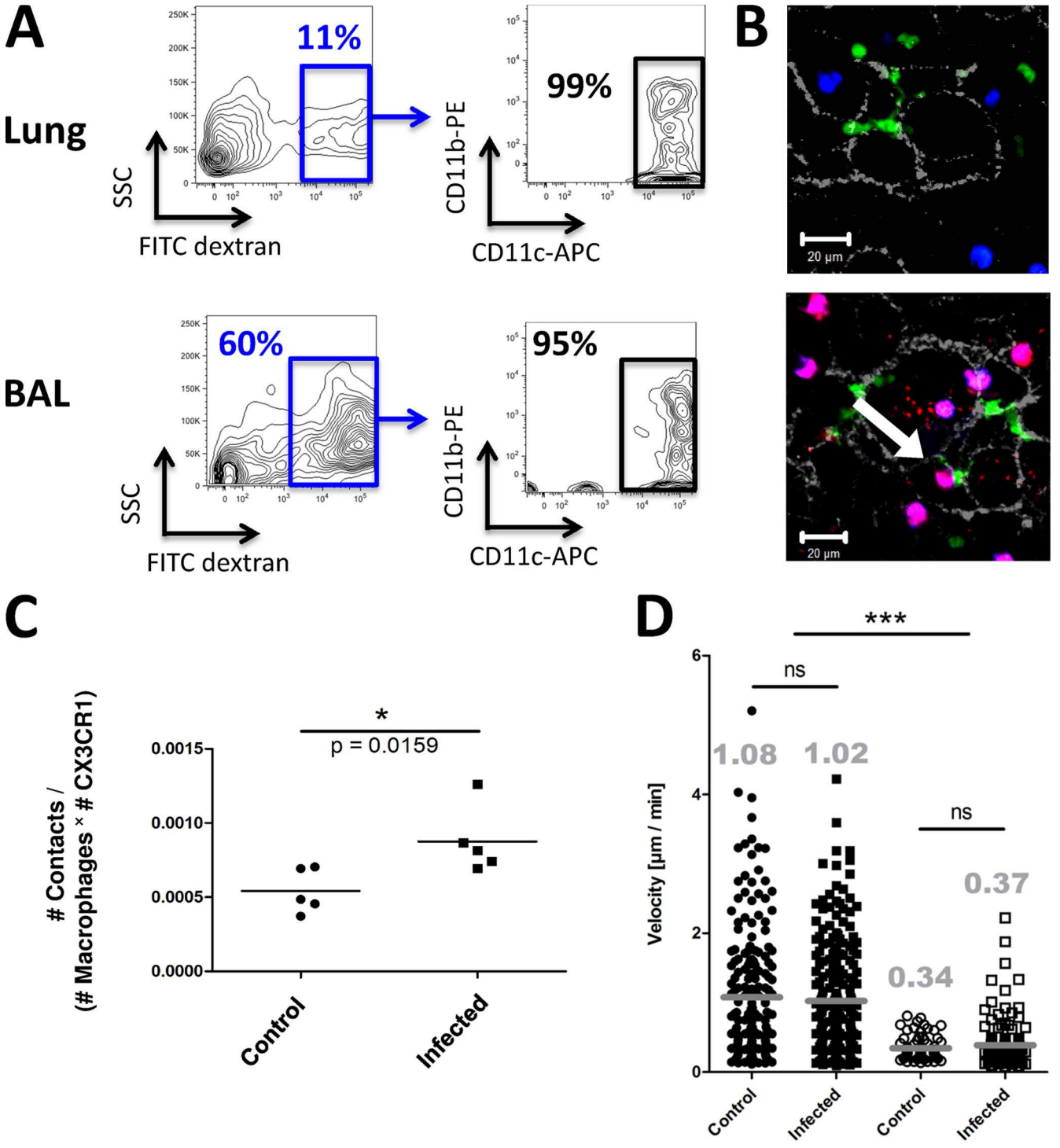

COLOR

FIG 3 Macrophage *in vivo* staining and statistical behavior. (A) Flow cytometry graphs performed on total lungs or bronchoalveolar lavage (BAL) fluid samples from mice administered FITC-dextran, gated on FITC-positive cells. Gray line, positive staining; black line, negative control. More than 95% of the dextran-loaded cells exhibited a CD11b-negative, CD11c-positive phenotype. All interpretations were performed after exclusion of doublet and dead cells. APC, allophycocyanin; PE, phycoerythrin; SSC, side scatter. (B) Projection of TPEF z-stacks performed *in situ* on naive (top panel) and infected (bottom panel) CX3CR1 mice. Green, CX3CR1 cells (GFP); red, *B. anthracis* spores (Alexa Fluor 633); blue, macrophages (rhodamine B-dextran); gray, fibrillar collagen (SHG). Spore-loaded macrophages appear in pink. The white arrow on the lower image highlights the contact between infected macrophage and a CX3CR1 cell. Bar, 20 µm. (C) Normalized ratio of CX3CR1 cell-macrophage contacts in control mice (PBS) and infected mice (spores). Each point represents the total number of contacts divided by the number of CX3CR1 cells and macrophages on 10 randomly chosen, *in situ* nonprojected z-stack determinations performed in the same mouse (five mice per group). (D) Velocity of CX3CR1 cells (filled symbols) and macrophages (open symbols) determined *in situ* from 5 to 6 h postinfection (squares) or injection of PBS (circles). Each point represents one cell, and there were three mice per group. Comparisons between groups were performed using the Mann-Whitney test and GraphPad Prism software (GraphPad Software, Inc.). *, P ●●●; **, P = ●●●; ns, nonsignificant.

AQ: B

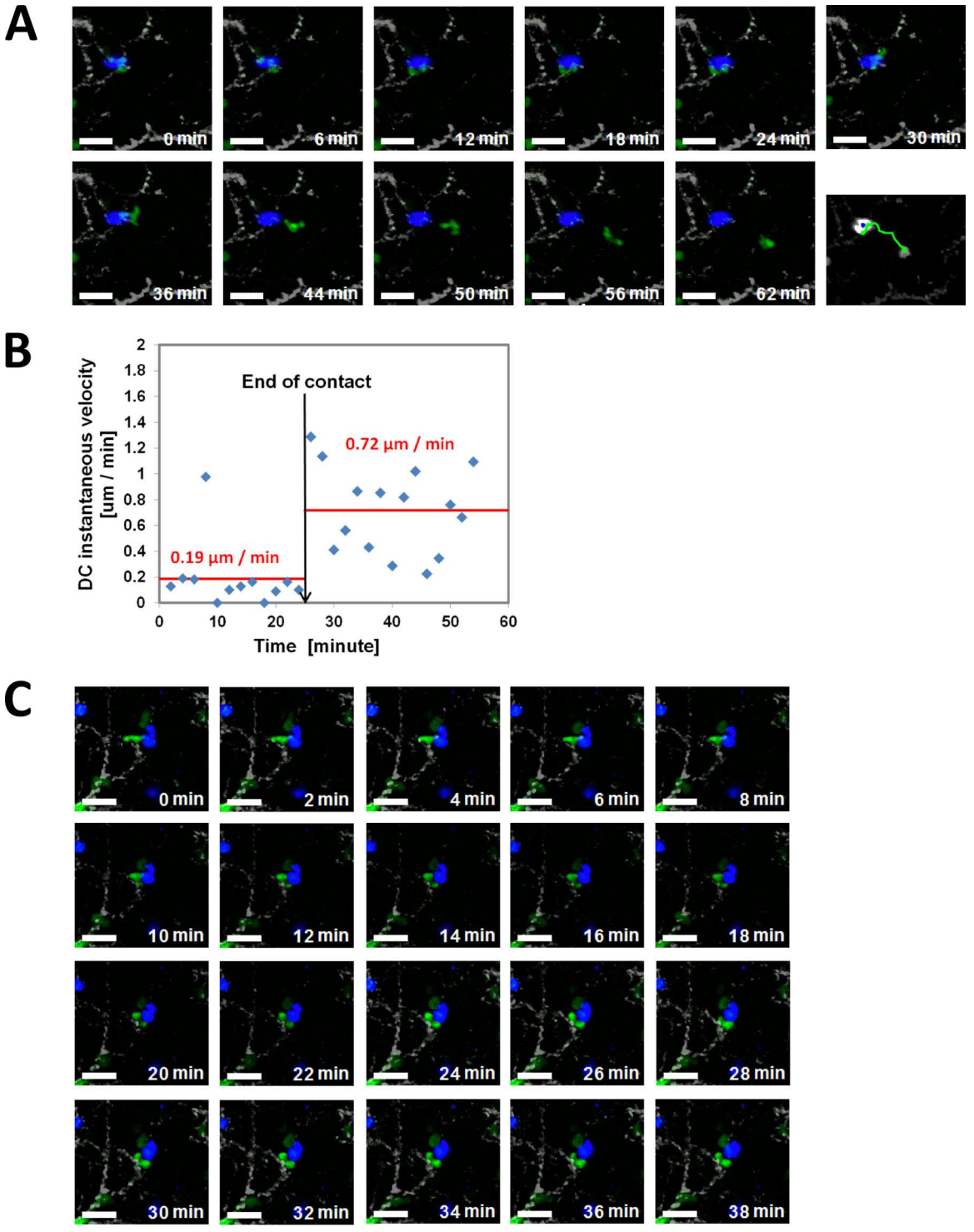

COLOR

FIG 4 *In situ* imaging of macrophage-DC contact after infection. (A) *In situ* TPEF z-projected time lapse of contact between a CX3CR1 cell and a macrophage from 5 to 6 h after infection by nonstained spores. The last frame shows the trajectories of a CX3CR1 cell (green line) and the macrophage (blue line) during the whole experiment (see Video S7 in the supplemental material). (B) Instantaneous velocity of the DC shown in panel A during and after contact. Average velocities during and after contact are shown in red. (C) Two CX3CR1 cells in contact with one macrophage 5 h after infection by nonstained spores (see Video S8 in the supplemental material). Green, CX3CR1 cells (GFP); blue, macrophages (rhodamine B-dextran); gray, fibrillar collagen (SHG). Bars, 10 µm.

these major immune cell populations when confronted by a bacterial pathogen. Our approach, based on postprocessing of time-oversampled acquisitions, utilizes SHG signal coming from fibrillar collagen as a reference for frame registration (Fig. 1). The main limitation of this method is that information from sample depth is lost due to unforeseeable chest motion, preventing 3D experiments. Future work could address this issue by synchronizing breathing and acquisition.

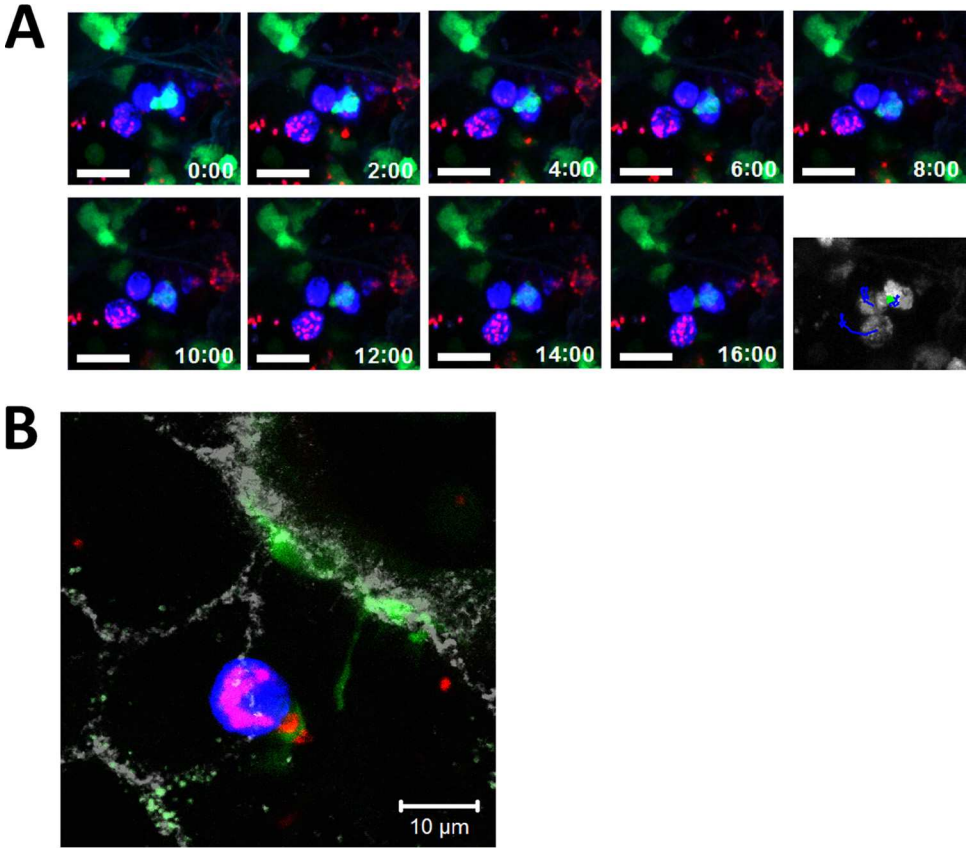

COLOR

FIG 5 *In situ* imaging of macrophage-DC contacts after infection with stained spores. (A) *In situ* confocal z-projected time lapse (in minutes) of infected macrophages and CX3CR1 cells 5 h after infection. Green, CX3CR1 cells (GFP); blue, macrophages (rhodamine B-dextran); red, *B. anthracis* spores (Alexa Fluor 633). Bar, 10 μm (see Video S9 in the supplemental material). (B) Projection of TPEF z-stack performed *in situ* for an infected CX3CR1 mouse. Green, CX3CR1 cells (GFP); red, *B. anthracis* spores (Alexa Fluor 633); blue, macrophage (rhodamine B-dextran); gray, fibrillar collagen (SHG). Bar, 10 μm.

This lung IVM method was combined with experiments performed on lung slices maintained under conditions favorable to cell dynamics. Precision-cut lung slices were prepared according to previously published procedures (27), with the exception that we did not fill the lungs with agarose (21). This method, allowing *in situ* imaging experiments, may avoid possible artifacts in alveolar cell behavior, making it more appropriate for the detection of slight immune cell displacements.

By using these methods on CX3CR1 mice, we have witnessed close interactions between *B. anthracis* spores and DCs not only *in situ* but also *in vivo* (Fig. 2 and 3). Because we were mostly interested in the early stage of spore capture (i.e., before germination), these results obtained with the acapsulated Sterne strain hold true for fully virulent strains. We did not observe any bacilli on our images, mainly because we chemically stained the exosporium that is lost during germination. It should be kept in mind that germination in the lung in this model is very rare. In our hands, we have never observed any significant level of germination in the lung (18, 28) by using Sterne strain in C57BL/6 mice. This is consistent with what is observed in immunocompetent mice by using bioluminescent strains (29).

Our observations led to two lines of thinking. First, the expected capture of spores by CX3CR1-DCs previously reported (19) appeared to be very scarce. Second, the synchronous motion of spores alongside the DC's surface (see Video S3 in the supplemental material), in addition to the gathering of multiple spores bordering DCs (Fig. 2A and C), strongly implies a previous capture of these spores by a CX3CR1-negative phagocyte. Specific *in vivo* staining of macrophages by rhodamine B (Fig. 3B) offered the possibility of simultaneous imaging of macrophages and GFP-expressing DCs after infection with Alexa Fluor-stained *B. anthracis* spores and imaging of fibrillar collagen by SHG detection. This multicolor imaging setup allowed a further statistical documentation of DC and macrophage populations following infection, revealing a significant increase of macrophage-DC contacts after infection (Fig. 3C). These data provide compelling evidence on the functional role of macrophage-DC contacts in the lung. Interestingly, the contact ratio increase does not appear to be correlated to any change in the speed of cell motion (Fig. 3D).

Taken together, these data require reexamination not only of the entry path of *B. anthracis* spores in the lungs but also of the role of cooperative interactions between macrophages and DCs.

After inhalation of *B. anthracis* spores, a fraction of spores enters the host immune system via the nose-associated lymphoid tissues (29, 30), while another fraction reaches the alveoli. They enter the host immune system via the draining lymph node, predominantly transported by DCs (2). In the lung at the cellular level, we have previously shown that alveolar macrophages capture spores within minutes in a first step, whereas DCs take over after 30 min and transport the spores to the lymph nodes (18).

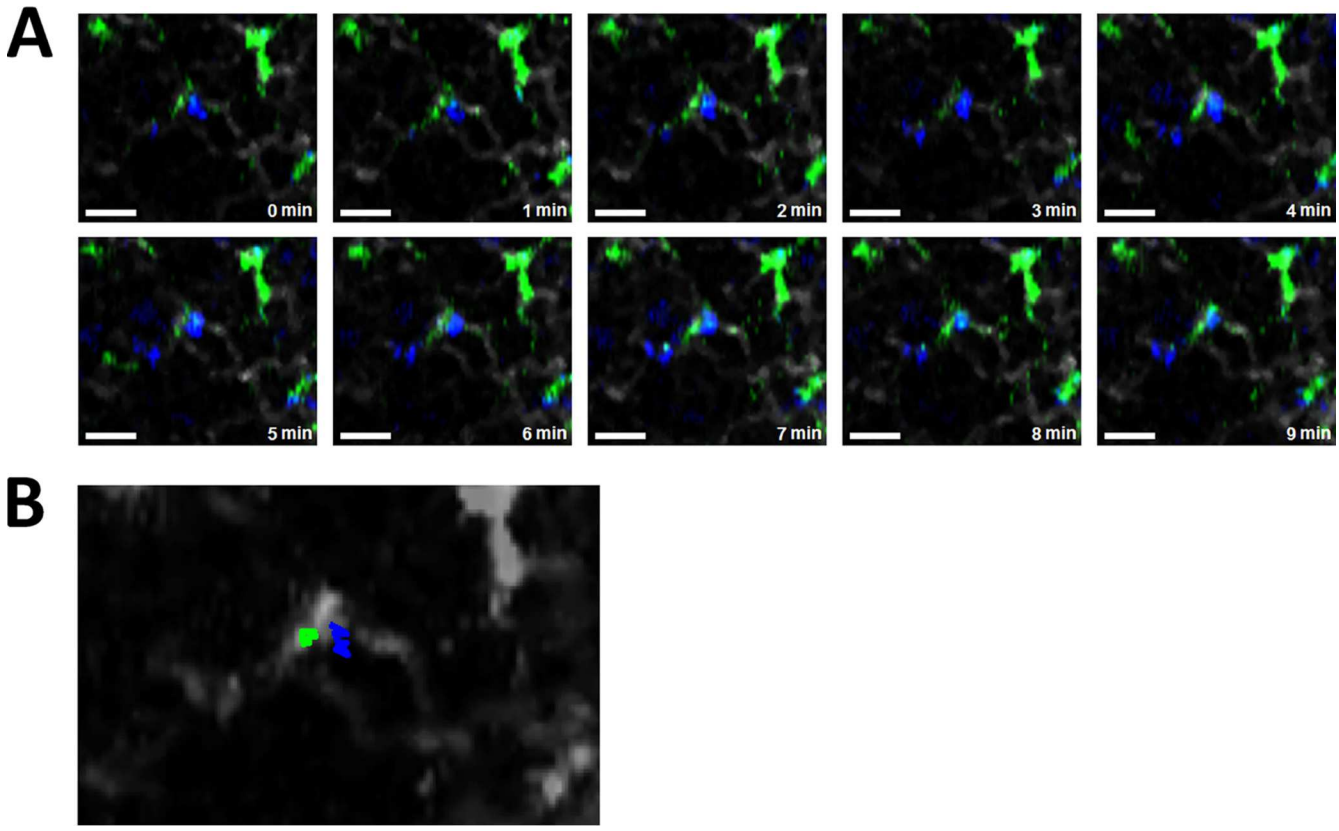

COLOR

FIG 6 *In vivo* imaging of macrophage-DC contacts after infection. (A) *In vivo* time lapse of macrophage-CX3CR1 cell interaction 5 h after infection by nonstained spores. Green, CX3CR1 cells (GFP); blue, macrophages (rhodamine B-dextran); gray, fibrillar collagen (SHG). Bar, 10 μm (see Video S10 in the supplemental material). (B) Trajectories of the CX3CR1 cell (green line) and the macrophage (blue line) during the whole experiment.

Until now, these two processes have appeared to be independent of one another. Our data tend to refine this model and demonstrate a cooperative role between macrophages and DCs. Upon triggering by the infection, the cross talk between macrophages and DCs may result in an exchange of information. Although we never observed spore transfer, it is plausible that macrophages and DCs exchange pathogen-derived particles *in vivo*, which could not be directly seen because of the spatial resolution of our system. Another option would be the exchange of exosomes containing pathogen-derived antigens released by macrophages directed to DCs. Exosomes are small (50-to-100-nm diameter) membrane vesicles secreted following the fusion of internal compartments known as multivesicular endosomes that can play the role of a vesicular carrier (31). Interestingly, exosomes from macrophages infected by *Mycobacterium bovis* BCG can activate bone marrow-derived DCs *in vitro* and $CD4^+$ and $CD8^+$ T cells *in vivo* (32). More recently, exosomes from *Mycobacterium tuberculosis*-infected macrophages administered intranasally have been used as a cell-free vaccine model (33). Still, we have observed what might be the last phase of spore transfer from macrophage to CX3CR1 cell (Fig. 5B). This mechanism was recently suggested *in vitro* (25) but, to our knowledge, has never been reported *in situ* or *in vivo*. Nevertheless, directed cytokine release or ligand-receptor triggering during long-duration (>30-min) contact between macrophage and DC is most likely and may impact the delicate balance between tolerance and immunity within the lung.

Synapses are defined as close cell-cell contacts whereby information is selectively transmitted. Immunological synapses were first described in the immune system at the interface between innate and adaptive cells, but the definition has recently been extended to NK cells and more recently to phagocytes (34). We have observed *in situ* and *in vivo* what may be a novel type of immunological synapse. The putative role of such synapse-like contacts between macrophages and DCs is still to be defined. However, infection leads to an increase of contact probability, suggesting that they play a role in the control of infection. Future investigations should clarify whether or not contacts occur due to chemotaxis by determining whether infection enhances the macrophage-DC contact ratio through an increase of contact duration or through an increase of contact probability.

This IVM-based study, which aimed to remove the need for mechanical stabilization of the lung and therefore diminish its invasiveness, highlights for the first time macrophage-DC contacts in this organ. These contacts may be the missing link for further understanding pathogen sampling by DCs through a triangular interaction between macrophages, DCs, and inhaled pathogens, eventually leading to the triggering of an adaptive immune response via an immunological synapse-like process.

ACKNOWLEDGMENTS

We thank Sarah Renault for the design of the thoracic window and Emily Martin and Bradley Stiles for reading and editing the manuscript.

This work was supported by the Direction Générale de l'Armement (DGA) [PDH-2-NRBC-4-B-203] and by the Agence Nationale pour la

Recherche [ANR-11-ASTR-022 01]. D.F. was supported by a fellowship from DGA.

REFERENCES

1. **Holt PG, Strickland DH, Wikström ME, Jahnsen FL.** 2008. Regulation of immunological homeostasis in the respiratory tract. Nat. Rev. Immunol. **8:**142–152. http://dx.doi.org/10.1038/nri2236.
2. **Tournier J-N, Mohamadzadeh M.** 2010. Key roles of dendritic cells in lung infection and improving anthrax vaccines. Trends Mol. Med. **16:**303–312. http://dx.doi.org/10.1016/j.molmed.2010.04.006.
3. **Lambrecht BN, Hammad H.** 2012. Lung dendritic cells in respiratory viral infection and asthma: from protection to immunopathology. Annu. Rev. Immunol. **30:**243–270. http://dx.doi.org/10.1146/annurev-immunol-020711-075021.
4. **Germain RN, Robey EA, Cahalan MD.** 2012. A decade of imaging cellular motility and interaction dynamics in the immune system. Science **336:**1676–1681. http://dx.doi.org/10.1126/science.1221063.
5. **Chtanova T, Han S-J, Schaeffer M, van Dooren GG, Herzmark P, Striepen B, Robey EA.** 2009. Dynamics of T cell, antigen-presenting cell, and pathogen interactions during recall responses in the lymph node. Immunity **31:**342–355. http://dx.doi.org/10.1016/j.immuni.2009.06.023.
6. **Filipe-Santos O, Pescher P, Breart B, Lippuner C, Aebischer T, Glaichenhaus N, Späth GF, Bousso P.** 2009. A dynamic map of antigen recognition by CD4 T cells at the site of Leishmania major infection. Cell Host Microbe **6:**23–33. http://dx.doi.org/10.1016/j.chom.2009.04.014.
7. **Chieppa M, Rescigno M, Huang AYC, Germain RN.** 2006. Dynamic imaging of dendritic cell extension into the small bowel lumen in response to epithelial cell TLR engagement. J. Exp. Med. **203:**2841–2852. http://dx.doi.org/10.1084/jem.20061884.
8. **Egen JG, Rothfuchs AG, Feng CG, Winter N, Sher A, Germain RN.** 2008. Macrophage and T cell dynamics during the development and disintegration of mycobacterial granulomas. Immunity **28:**271–284. http://dx.doi.org/10.1016/j.immuni.2007.12.010.
9. **Hickman HD, Takeda K, Skon CN, Murray FR, Hensley SE, Loomis J, Barber GN, Bennink JR, Yewdell JW.** 2008. Direct priming of antiviral CD8+ T cells in the peripheral interfollicular region of lymph nodes. Nat. Immunol. **9:**155–165. http://dx.doi.org/10.1038/ni1557.
10. **John B, Harris TH, Tait ED, Wilson EH, Gregg B, Ng LG, Mrass P, Roos DS, Dzierszinski F, Weninger W, Hunter CA.** 2009. Dynamic imaging of CD8(+) T cells and dendritic cells during infection with Toxoplasma gondii. PLoS Pathog. **5:**e1000505. http://dx.doi.org/10.1371/journal.ppat.1000505.
11. **Egen JG, Rothfuchs AG, Feng CG, Horwitz MA, Sher A, Germain RN.** 2011. Intravital imaging reveals limited antigen presentation and T cell effector function in mycobacterial granulomas. Immunity **34:**807–819. http://dx.doi.org/10.1016/j.immuni.2011.03.022.
12. **Bhattacharya J.** 2011. Seeing is believing. Nat. Methods **8:**57–58. http://dx.doi.org/10.1038/nmeth0111-57.
13. **Kreisel D, Nava RG, Li W, Zinselmeyer BH, Wang B, Lai J, Pless R, Gelman AE, Krupnick AS, Miller MJ.** 2010. In vivo two-photon imaging reveals monocyte-dependent neutrophil extravasation during pulmonary inflammation. Proc. Natl. Acad. Sci. U. S. A. **107:**18073–18078. http://dx.doi.org/10.1073/pnas.1008737107.
14. **Looney MR, Thornton EE, Sen D, Lamm WJ, Glenny RW, Krummel MF.** 2011. Stabilized imaging of immune surveillance in the mouse lung. Nat. Methods **8:**91–96. http://dx.doi.org/10.1038/nmeth.1543.
15. **Thornton EE, Looney MR, Bose O, Sen D, Sheppard D, Locksley R, Huang X, Krummel MF.** 2012. Spatiotemporally separated antigen uptake by alveolar dendritic cells and airway presentation to T cells in the lung. J. Exp. Med. **209:**1183–1199. http://dx.doi.org/10.1084/jem.20112667.
16. **Goossens PL.** 2009. Animal models of human anthrax: the quest for the Holy Grail. Mol. Aspects Med. **30:**467–480. http://dx.doi.org/10.1016/j.mam.2009.07.005.
17. **Tournier J-N, Quesnel-Hellmann A, Cleret A, Vidal DR.** 2007. Contribution of toxins to the pathogenesis of inhalational anthrax. Cell. Microbiol. **9:**555–565. http://dx.doi.org/10.1111/j.1462-5822.2006.00866.x.
18. **Cleret A, Quesnel-Hellmann A, Vallon-Eberhard A, Verrier B, Jung S, Vidal D, Mathieu J, Tournier J-N.** 2007. Lung dendritic cells rapidly mediate anthrax spore entry through the pulmonary route. J. Immunol. **178:**7994–8001.
19. **Fiole D, Douady J, Vial J-C, Quesnel-Hellmann A, Tournier J-N.** 2012. Dynamics of rapid spore capture by dendritic cells in the lung alveolus. Am. J. Respir. Crit. Care Med. **186:**e2–e3. http://dx.doi.org/10.1164/rccm.201110-1782IM.
20. **Thornton EE, Krummel MF, Looney MR.** 2012. Live imaging of the lung. Curr. Protoc. Cytom. **60:**12.28.1–12.28.12. http://dx.doi.org/10.1002/0471142956.cy1228s60.
21. **Fiole D, Touvrey C, Quesnel-Hellmann A, Douady J, Tournier J-N.** 2012. Shape-based tracking allows functional discrimination of two immune cell subsets expressing the same fluorescent tag in mouse lung explant. PLoS One **7:**e39831. http://dx.doi.org/10.1371/journal.pone.0039831.
22. **Veres TZ, Zoltán Veres T, Voedisch S, Spies E, Tschernig T, Braun A.** 2011. Spatiotemporal and functional behavior of airway dendritic cells visualized by two-photon microscopy. Am. J. Pathol. **179:**603–609. http://dx.doi.org/10.1016/j.ajpath.2011.04.039.
23. **Presson RG, Jr, Brown MB, Fisher AJ, Sandoval RM, Dunn KW, Lorenz KS, Delp EJ, Salama P, Molitoris BA, Petrache I.** 2011. Two-photon imaging within the murine thorax without respiratory and cardiac motion artifact. Am. J. Pathol. **179:**75–82. http://dx.doi.org/10.1016/j.ajpath.2011.03.048.
24. **Mlodzianoski MJ, Schreiner JM, Callahan SP, Smolková K, Dlasková A, Santorová J, Ježek P, Bewersdorf J.** 2011. Sample drift correction in 3D fluorescence photoactivation localization microscopy. Opt. Express **19:**15009–15019. http://dx.doi.org/10.1364/OE.19.015009.
25. **Blank F, Wehrli M, Lehmann A, Baum O, Gehr P, von Garnier C, Rothen-Rutishauser BM.** 2011. Macrophages and dendritic cells express tight junction proteins and exchange particles in an in vitro model of the human airway wall. Immunobiology **216:**86–95. http://dx.doi.org/10.1016/j.imbio.2010.02.006.
26. **Nava RG, Li W, Gelman AE, Krupnick AS, Miller MJ, Kreisel D.** 2010. Two-photon microscopy in pulmonary research. Semin. Immunopathol. **32:**297–304. http://dx.doi.org/10.1007/s00281-010-0209-9.
27. **Henjakovic M, Sewald K, Switalla S, Kaiser D, Müller M, Veres TZ, Martin C, Uhlig S, Krug N, Braun A.** 2008. Ex vivo testing of immune responses in precision-cut lung slices. Toxicol. Appl. Pharmacol. **231:**68–76. http://dx.doi.org/10.1016/j.taap.2008.04.003.
28. **Garraud K, Cleret A, Mathieu J, Fiole D, Gauthier Y, Quesnel-Hellmann A, Tournier J-N.** 2012. Differential role of the interleukin-17 axis and neutrophils in resolution of inhalational anthrax. Infect. Immun. **80:**131–142. http://dx.doi.org/10.1128/IAI.05988-11.
29. **Glomski IJ, Piris-Gimenez A, Huerre M, Mock M, Goossens PL.** 2007. Primary involvement of pharynx and Peyer's patch in inhalational and intestinal anthrax. PLoS Pathog. **3:**e76. http://dx.doi.org/10.1371/journal.ppat.0030076.
30. **Dumetz F, Jouvion G, Khun H, Glomski IJ, Corre J-P, Rougeaux C, Tang W-J, Mock M, Huerre M, Goossens PL.** 2011. Noninvasive imaging technologies reveal edema toxin as a key virulence factor in anthrax. Am. J. Pathol. **178:**2523–2535. http://dx.doi.org/10.1016/j.ajpath.2011.02.027.
31. **Théry C, Ostrowski M, Segura E.** 2009. Membrane vesicles as conveyors of immune responses. Nat. Rev. Immunol. **9:**581–593. http://dx.doi.org/10.1038/nri2567.
32. **Giri PK, Schorey JS.** 2008. Exosomes derived from M. bovis BCG infected macrophages activate antigen-specific CD4+ and CD8+ T cells in vitro and in vivo. PLoS One **3:**e2461. http://dx.doi.org/10.1371/journal.pone.0002461.
33. **Cheng Y, Schorey JS.** 14 August 2013. Exosomes carrying mycobacterial antigens can protect mice against Mycobacterium tuberculosis infection. Eur. J. Immunol. http://dx.doi.org/10.1002/eji.201343727.
34. **Dustin ML.** 2012. Signaling at neuro/immune synapses. J. Clin. Invest. **122:**1149–1155. http://dx.doi.org/10.1172/JCI58705.